Shock Tube Study of the Oxidation of C_3F_6 by N_2O

Robert G. Hynes,*,† John C. Mackie,*,† and Assaad R. Masri‡

School of Chemistry and Department of Mechanical and Mechatronic Engineering, University of Sydney, NSW 2006, Australia

Received: March 26, 1999; In Final Form: May 19, 1999

The kinetics of the high-temperature oxidation of C_3F_6 by $O(^3P)$ have been studied by experiment, using a single-pulse shock tube, and by kinetic modeling. The O atoms were generated by the thermal decomposition of N_2O. Three mixtures, each diluted in argon, were studied: 0.6 mol % of C_3F_6 with 1.5 mol % N_2O; 6.2 mol % of C_3F_6 with 0.6 mol % of N_2O; and 6.3 mol % of N_2O and 0.7 mol % of C_3F_6. The temperatures were in the range 1300−1600 K, the residence times behind the reflected shock were in the range 550−850 μs, and the pressures were between 16 and 20 atm. Fluorinated products have been quantified with gas chromatography, oxidized products with Fourier transform infrared spectroscopy; identification of unknown fluorocarbons has been performed with gas chromatography−mass spectrometry. The most significant products detected were C_2F_6, C_2F_4, CF_2O, CO, CO_2, and CF_4. A detailed kinetic scheme is presented to model the experimental reactant and product yields as a function of temperature. Modeling showed that O-addition to either carbon of the double bond of C_3F_6 occurs. The rate constant for O-addition to the terminal carbon of the double bond, $C_3F_6 + O(^3P) \rightarrow {}^3CF_3CF + CF_2O$, was deduced to be $k_{71} = 10^{12.7}T^{0.05}\exp(-0.4\text{ kJ mol}^{-1}/RT)$ cm^3 mol^{-1} s^{-1}, and for addition to the central carbon, $C_3F_6 + O(^3P) \rightarrow CF_3 + CF_2CF{=}O$, $k_{72} = 10^{12.5}$ cm^3 mol^{-1} s^{-1}. Under oxidizer-rich conditions, ignition of the C_3F_6 occurred. Rate of production analyses showed that ignition was propagated by an F atom chain involving the $CF_2 + O$ and unimolecular CFO decomposition reactions. Under C_3F_6-rich conditions, single- and double-bond pyrolysis were the important destruction routes.

Introduction

Hydrofluorocarbons such as 2-H heptafluoropropane, CF_3CHFCF_3, have become viable alternatives to ozone-depleting halons for flame inhibition. Recent flame[1] and shock tube[2] studies on 2-H heptafluoropropane show that an important product of inhibitor decomposition is C_3F_6, produced by the 1,2 elimination of HF. Since the flame chemistry of C_3F_6 is uncertain at present, it is of interest to study in detail the high-temperature oxidation of C_3F_6. For this purpose, the thermal decomposition of N_2O is used to produce O atoms. The advantage of using N_2O is that it begins to decompose and liberate O atoms at temperatures well below those required for pyrolysis of C_3F_6. Thus, at least for temperatures below the onset of pyrolysis, N_2O should be a useful precursor of O atoms to study the reactions between these atoms and C_3F_6.

To date, little is known of the O atom addition kinetics to unsaturated fluorocarbons at high temperatures. Heicklen and Saunders[3] previously studied addition of O to C_3F_6 at room temperature, using the mercury-sensitized decomposition of N_2O as a source of O atoms. An important observation was that CF_2O was a major product and the CF_3CFO yield was substantially less. The rate constant for the reaction of O with C_3F_6 producing CF_2O and $CF_3\ddot{C}F$, measured in competition with C_2H_4, was found to be 2.1×10^{10} cm^3 mol^{-1} s^{-1} at 297 K. The other O-addition channel producing CF_3CFO and CF_2 in an assumed triplet state was found to be 6.5 times slower than that which produces CF_2O.

In the case of C_2F_4, there is also a lack of high-temperature (i.e., above 500 K) kinetic data for O atom addition. A recent $C_2F_4-O_2$ flame study[4] utilizes an O-atom addition rate constant of $8.13 \times 10^{12}\exp(-5.3\text{ kJ mol}^{-1}/RT)$ cm^3 mol^{-1} s^{-1}. However, this rate constant cannot be used as an analogy for the $C_3F_6 + O(^3P)$ reaction because the latter reaction would be expected to have two channels: addition to the central carbon atom, which might be expected to form CF_3CFO and triplet CF_2, and addition to the terminal carbon, which should lead to triplet $CF_3\ddot{C}F$ carbene (initially) and CF_2O.

Therefore, the purpose of this work is to study the oxidation of C_3F_6 in the presence of N_2O. By measuring stable product yields as a function of initial concentration of reactants and temperature and comparing these yields to numerically modeled profiles, the rate constants for the addition of O atoms to C_3F_6 can be deduced. The rate constants for other secondary processes will also be determined.

Experimental Section

Quantification of the reactants and the fluorinated products is carried out with a Hewlett-Packard 6890 gas chromatograph equipped with a 25 m SGE-BP1 column (5 μm film thickness) operated isothermally at −20 °C. Detection was by FID. N_2O, O_2, and N_2 were quantified using the same GC equipped with a HP PLOT Molecular Sieve 5A column, operated with a temperature program of −10 °C isothermal for 7 min, then ramped up to 200 °C to elute the N_2O. Detection was by TCD.

In this work, the oxidation of hexafluoropropene was studied diluted in argon in three concentration ranges. First, the decomposition of a near-stoichiometric mixture of 0.6 mol % C_3F_6 and 1.5 mol % N_2O was studied. In the second study, a

* Corresponding authors. E-mail for RGH: hynes_r@chem.usyd.edu.au. E-mail for JCM: j.mackie@chem.usyd.edu.au. Fax: 61-2-9351-3329.
† School of Chemistry.
‡ Department of Mechanical and Mechatronic Engineering.

10.1021/jp991065v CCC: $18.00
Published on Web 07/09/1999

large excess of N_2O was used, 6.3 mol % N_2O with 0.7% C_3F_6. Third, an excess amount of C_3F_6, 6.2 mol %, was reacted with 0.6 mol % of N_2O. The assumed stoichiometry of this reaction (to be discussed later) is

$$C_3F_6 + 3N_2O \rightarrow CF_2O + CF_4 + CO_2 + 3\,N_2$$

The diluent gas was argon (British Oxygen Corporation Gases 99.995%; minimum purity). Pure hexafluoropropene (Mathesons; 99+ % purity) was analyzed by GC and showed no impurities; it was used without purification. The nitrous oxide (British Oxygen Corporation Gases; 99.5% mimimum purity) was similarly analyzed. An atmosphere of the N_2O showed small traces of N_2 (0.25%) and O_2 (0.066%). When used diluted, these two impurities were undetectable by GC. A preshock GC analysis (using both thermal conductivity and flame ionization detection) of the $C_3F_6/N_2O/Ar$ reactant mixture did not reveal the presence of any significant impurities.

The pressure and temperature behind the reflected shock were calculated from the measured incident and reflected shock velocities. Residence times were obtained from the pressure profiles measured using Kistler pressure transducers. Signals were then collected by a Tektronix TDS 430A two-channel digitizing oscilloscope. Experiments with excess N_2O were performed over the temperature range 1300−1550 K, while experiments with excess C_3F_6 were performed over the range 1400−1650 K. Typical residence times behind the reflected shocks were 550−850 μs, with pressures between 16 and 20 atm. The excess C_3F_6 runs had residence times that were shorter than the excess N_2O runs by ∼100 μs.

Quantification of fluorocarbons was performed by measuring the FID response for C_2F_6 (Sigma-Aldrich; 98+% purity) and C_3F_6. The FID response of C_2F_4, for which calibration samples were not available, was assumed to be 0.667 of the response of C_3F_6 on a molar basis. FTIR analysis was performed by taking ∼100 Torr of the reaction mixture and diluting it with argon to 1 atm. Sample CO and CO_2 concentrations were determined by comparing infrared peak areas with those of a gas mixture (Scotty Specialty Gases, Mix 216) containing 1.00 ± 0.02% of the said gases in nitrogen. Where sample concentrations were less than 1%, a second mixture (British Oxygen Corp. Gases, Special Beta Mixture) containing ∼420 ppm of CO and CO_2 in N_2 was used. Sample CF_4 concentrations were determined by comparing sample IR peak areas with those samples of the pure compound (Mathesons 99.9% purity) diluted in argon. CF_2O was quantified by comparing sample peak areas with those from a standard spectrum obtained at the same resolution and same total pressure. All spectra were measured at a total pressure of 1 atm with an instrument resolution of 0.5 cm^{-1}. FTIR calibration for CF_3CFO (Fluorochem. Ltd.; 96.3% purity; impurities due to CF_3CClO and traces of acetic acid) was performed using small concentrations of the gas in argon. Identification of heavier products was performed with a Hewlett-Packard 5890 II GC interfaced with a Hewlett-Packard 5898A MS Engine, equipped with an SGE-BP1 column and operated isothermally at −60 °C.

Results and Discussion

1. Mixtures of 0.6 mol % C_3F_6 and 1.5 mol % N_2O (Near Stoichiometric). Elemental carbon, oxygen, fluorine, and nitrogen mass balances of unconsumed reactants and recovered products in all sets were generally of the order of 100 ± 10% for temperatures of ≤1500 K. At temperatures above 1560 K, the fluorine and carbon recovery dropped to 80% suggesting the formation of higher molecular weight fluorocarbons, including polymers. However, polymers were not detected in the gas samples.

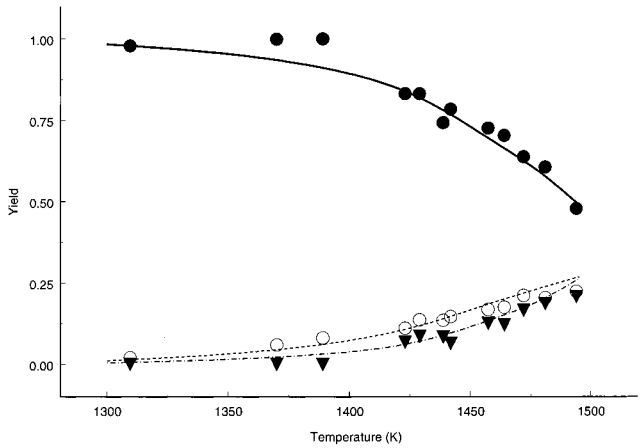

Figure 1. Variation with temperature of the experimental C_3F_6, C_2F_4, and C_2F_6 yields. The respective experimental points are represented by the symbols (●, ○, ▼); model profiles are indicated by the lines: (—, - - -, - — -). Initial mixture: 0.6 mol % C_3F_6 and 1.5 mol % N_2O.

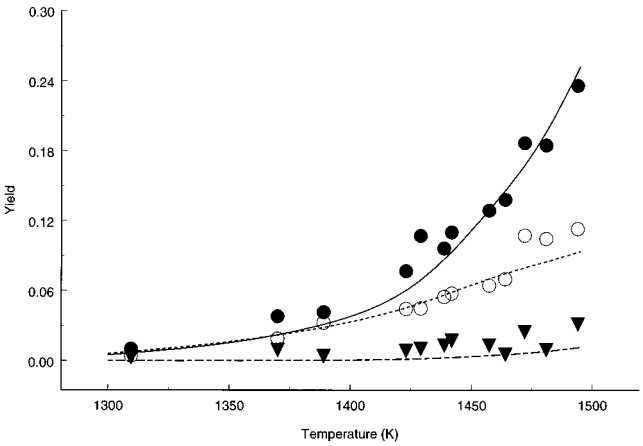

Figure 2. Variation with temperature of the experimental CO, CF_2O, and CO_2 yields. The respective experimental points are represented by the symbols (●, ○, ▼); model profiles are indicated by the lines: (—, - - -, - — -). Initial mixture: 0.6 mol % C_3F_6 and 1.5 mol % N_2O.

Figures 1−3 show profiles of product yields versus the frozen reflected shocked gas temperature. Yields for nitrogen-containing species are based on the initial N_2O concentration, whereas yields for fluorocarbon and partially and fully oxidized species are based on the initial C_3F_6 concentration. Figure 1 shows that significant C_3F_6 decomposition occurs at temperatures above 1400 K. To verify that this was not due to pyrolysis, a small number of runs was performed with 0.6 mol % C_3F_6 in argon. These experiments showed that pyrolysis is significant only above 1600 K. This result is in accord with the C_3F_6 pyrolysis study of Bauer et al.[5] The yields of C_2F_4 and C_2F_6 were similar at temperatures up to 1500 K. The maximum yield of both species at 1500 K was 0.25. The most significant of the oxidized products was CO. At 1500 K, the yield of CO was 0.24 compared with the CF_2O yield of 0.12 and the CO_2 yield of only 0.03. An important observation was that CF_3CFO was not detected in any of the runs. This suggests that the room-temperature oxidation route proposed by Saunders and Heicklen[3] is inappropriate at high temperatures. Small quantities of NO were formed. However, quantification of this species was difficult due to its low absorption coefficient and hence low signal-to-noise ratio. Subtracting C_3F_6, CF_2O, and N_2O signals

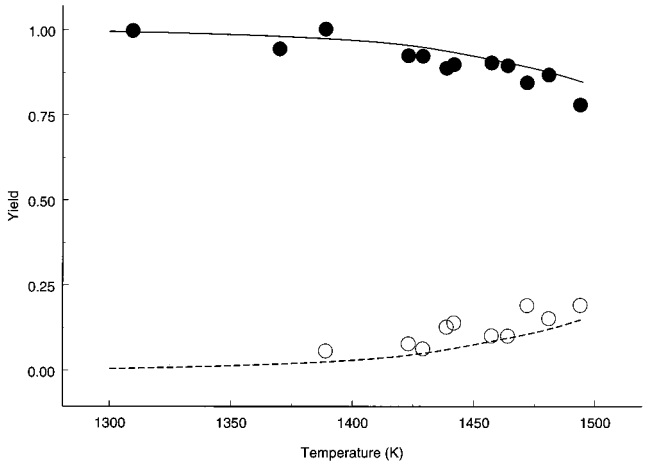

Figure 3. Variation with temperature of the experimental N_2O and N_2 yields. The respective experimental points are represented by the symbols (●, ○); model profiles are indicated by the lines: (—, - - -). Initial mixture: 0.6 mol % C_3F_6 and 1.5 mol % N_2O.

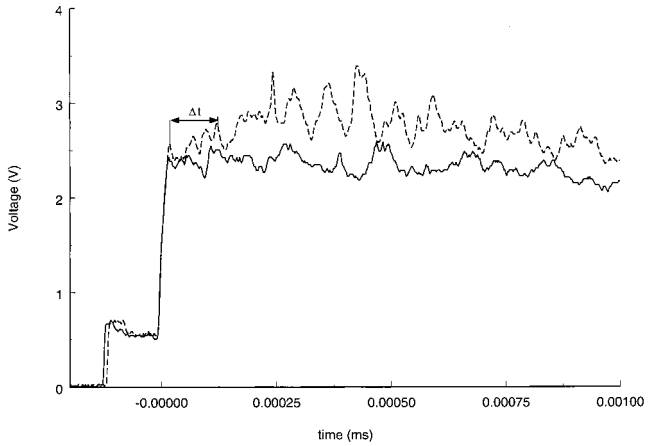

Figure 4. Variation with time of the experimental pressure profiles. For the vertical scale, 10 mV = 1 PSI (0.07 atm). The lines (—, - - -) refer to a pre-ignition run (1440 K) and a post-ignition run (1540 K), respectively. Initial mixture: 0.7 mol % C_3F_6 and 6.3 mol % N_2O.

from the product FTIR spectra did not reveal the presence of any other significant species. Other species such as CF_3NO,[6] CF_3OF,[7] and FNO[8] were searched for but not detected in the infrared spectra. This is also true of the other two sets of experiments to be discussed below.

Arrhenius plots of the rate of disappearance of N_2O and C_3F_6 and the rate of appearance of CF_2O showed that the activation energy for N_2O and C_3F_6 decomposition and CF_2O formation were very similar. This indicates that the rate-determining step in this series was the decomposition of N_2O to form O atoms.

Figure 3 shows a plot of N_2O and N_2 yields versus temperature. These were the only significant nitrogenous compounds detected in the product mixtures. At 1500 K, only 20% of the initial N_2O has decomposed, with the principal nitrogenous product being N_2. NO_2 was not detected in any of the infrared spectra, and the NO was found in insignificant concentrations.

2. Mixtures of 0.7 mol % C_3F_6 and 6.3 mol % N_2O (Excess Oxidant). The oxidation process in this series was found to differ considerably from that described in the first series. Over the temperature range 1300−1400 K, the behavior of the two series is similar. Above 1410 K, *ignition* of the C_3F_6 was observed along with the production of significant quantities of CF_4 and O_2. NO and NO_2 were observed; however, because of the presence of O_2 in the products, secondary oxidation occurred within the infrared cell, making the quantification of these species difficult. A good indication that ignition had indeed occurred is given by comparing shock tube pressure traces at temperatures above and below the ignition temperature. The variation of pressure with time is shown in Figure 4. The post-ignition run reaches a higher pressure, ∼20.5 atm, compared with the pre-ignition run which reached 16.5 atm. The oscillations in the post-ignition run may be due to detonation effects or acoustic waves travelling in the body of the shock tube. Kinetic modeling (discussed below) did not support the possibility of oscillating kinetics. The Δt in the figure refers to the ignition delay, which is measured to be 240 ± 50 μs where the initial shocked gas temperature is 1540 K.

Figure 5 shows yield versus temperature plots for C_3F_6, C_2F_4, and C_2F_6. Unlike the first series, the C_3F_6 is completely decomposed when the initial reflected shocked gas temperature is above 1450 K. The C_2F_4 and C_2F_6 profiles show a steady increase up until 1430 K, after which, the C_2F_4 yield drops to zero at 1450 K. However, the C_2F_6 shows a sharp increase, as

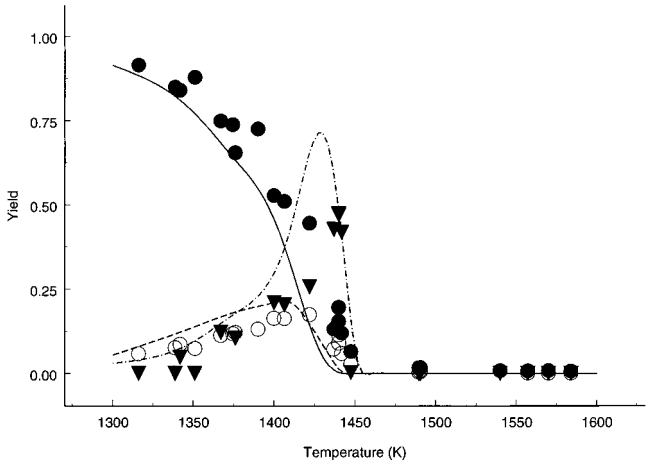

Figure 5. The variation with temperature of the experimental C_3F_6, C_2F_4, and C_2F_6 yields. The respective experimental points are represented by the symbols (●, ○, ▼); model profiles are indicated by the lines: (—, - - -, - — -). Initial mixture: 0.7 mol % C_3F_6 and 6.3 mol % N_2O.

presumably more CF_3 becomes available for recombination. Above an initial temperature of 1450 K, both the C_2F_4 and C_2F_6 profiles drop to zero. Figure 6 shows the profiles of CF_2O, CO, and CO_2. Above 1450 K, a CF_2O yield of 0.9 was obtained; CO and CO_2 yields were 0.5 and 0.3, respectively. This is different from the previous series where the major partially oxidized product was CO. Product yields show a large increase above the temperature for ignition. Figure 7 shows the profile of CF_4 (max. yield of ∼1.0) and O_2. The appearance of CF_4 at temperatures above 1450 K is related to the appearance of the spike in the C_2F_6 profile. This is again due to the large increase in concentration at 1450 K of CF_3 radicals, which recombine to yield C_2F_6. The appearance of CF_4 suggests the presence of a large concentration of F atoms which are terminated by recombination with CF_3. The kinetics of the ignition process will be discussed in the numerical modeling section. Figure 8 shows the yield profiles for N_2O and N_2. This plot shows that above 1450 K the N_2O has almost entirely decomposed to N_2. As mentioned above, NO and NO_2 were observed in the product mixture, with maximum measured yields of ∼0.1 each. Secondary reactions involving NO and O_2 within the infrared cell prevented accurate concentration measurements, and these are not reported in this work.

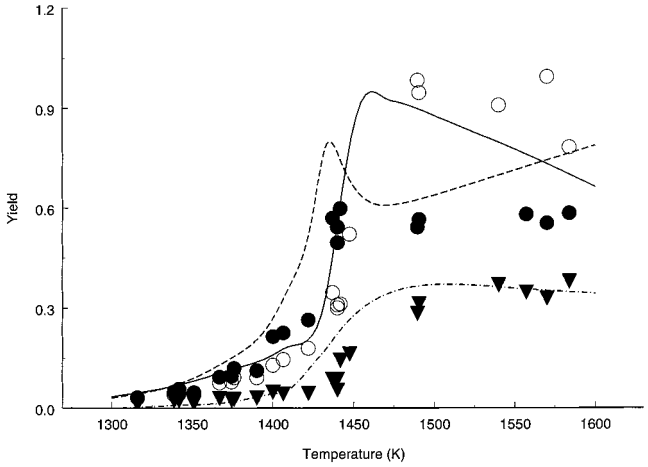

Figure 6. Variation with temperature of the experimental CO, CF_2O, and CO_2 yields. The respective experimental points are represented by the symbols (●, ○, ▼); model profiles are indicated by the lines: (—, - - -, - — -). Initial mixture: 0.7 mol % C_3F_6 and 6.3 mol % N_2O.

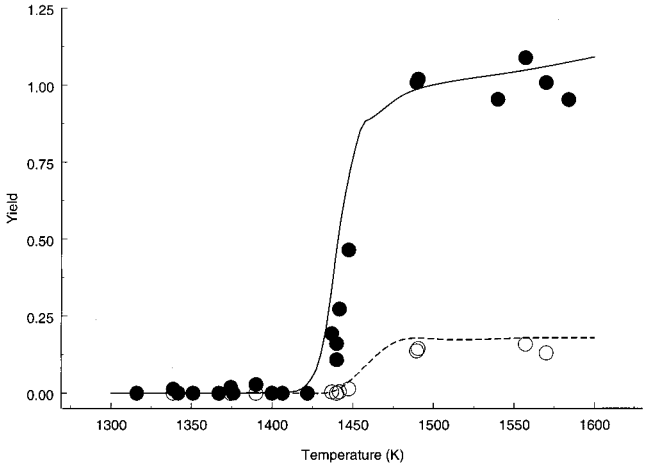

Figure 7. Variation with temperature of the experimental CF_4 and O_2 yields. The respective experimental points are represented by the symbols (●, ○); model profiles are indicated by the lines: (—, - - -). Initial mixture: 0.7 mol % C_3F_6 and 6.3 mol % N_2O.

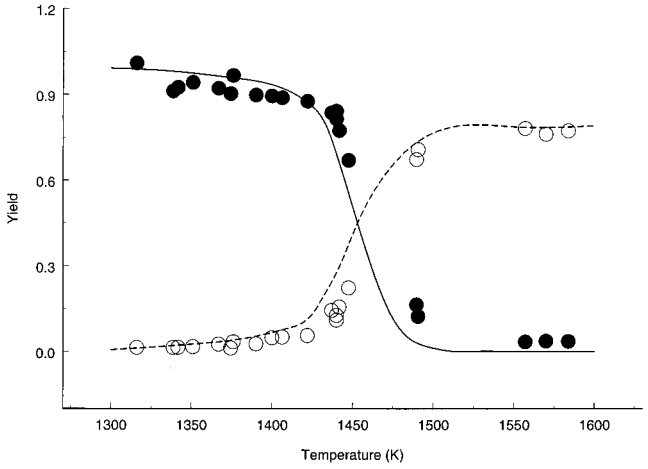

Figure 8. Variation with temperature of the experimental N_2O and N_2 yields. The respective experimental points are represented by the symbols (●, ○); model profiles are indicated by the lines: (—, - - -). Initial mixture: 0.7 mol % C_3F_6 and 6.3 mol % N_2O.

In terms of the stoichiometry proposed above for the C_3F_6 oxidation, the measured yields of ~1.0 for both CF_4 and CF_2O are consistent. Further, these two products are the major sinks for F atoms at equilibrium. The stoichiometry predicts a yield of 1.0 for CO_2; experimentally, CO and CO_2 are both observed with a combined yield of 0.8. This indicates that, at 1600 K, partial, rather than complete, oxidation to CO_2 is occurring.

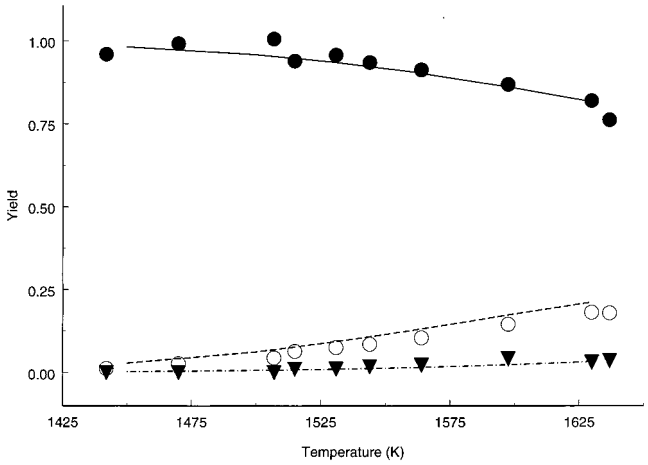

Figure 9. Variation with temperature of the experimental C_3F_6, C_2F_4, and C_2F_6 yields. The respective experimental points are represented by the symbols (●, ○, ▼); model profiles are indicated by the lines: (—, - - -, - — -). Note that the C_2F_4 yields have been multiplied by 2 for clarity. Initial mixture: 6.2 mol % C_3F_6 and 0.6 mol % N_2O.

3. Mixtures of 6.2 mol % C_3F_6 and 0.6 mol % N_2O (Fuel Rich). This series also shows somewhat different decomposition characteristics from the previous two series. As there is a large excess of C_3F_6 in the mixture, it is expected that some pyrolysis will occur. Figure 9 shows the variation with temperature of the C_3F_6, C_2F_4, and C_2F_6 yields. At a temperature of 1640 K, only 20−25% of the C_3F_6 has decomposed. The major products of decomposition in this series are C_2F_4 (maximum yield at 1640 K of ~0.09) and C_2F_6 (0.035). Note in Figure 9 that the C_2F_4 yields have been multiplied by two for clarity. GC-MS was used to detect heavier fluorocarbon compounds in this series, and the two most important were *iso*-C_4F_8 ($CF_2{=}CF(CF_3)_2$) and 2-C_4F_8 ($CF_3CF_2{=}CF_2CF_3$). The maximum yields of each of these species at 1640 K were 0.025 and 0.011, respectively. Other heavier fluorocarbons include octafluoropropane, C_4F_6 (identified as hexafluoro-2-butyne), perfluorinated cyclobutenes, hexafluorobenzene, pentafluorocyclopentadiene, and pentafluoro(trifluoromethyl)benzene. Figure 10 shows the CF_2O, CO, and CO_2 product yields. Note that both the CF_2O and CO_2 yields have been multiplied by two for clarity. The yields of these species are quite low with the maximum CF_2O yield of 0.018 at 1640 K. The yields of CO and CO_2 at this temperature were 0.017 and 0.0015, respectively. The yields of the two C_4F_8 isomers are consistently low in all three sets of experiments. Figure 11 shows the N_2O and N_2 profiles where essentially all of the nitrogen in the N_2O is converted to N_2. Small yields (<0.01) of NO and NO_2 were detected in the infrared spectra. In the presence of a large excess of O_2, NO may be oxidized to NO_2 in the infrared cell and the appearance of the NO_2 may be an artifact. This oxidation of NO is supported by the loss of O_2 at temperatures where more O_2 is expected and by the low levels of NO recorded. Thus, the NO and NO_2 measurements are not reliable and are not reported here. Also, no CF_3CFO was detected in any of the product gas samples.

The Reaction Model. A 77-step reaction model with 38 species was assembled in this work to model the oxidation of C_3F_6, as summarized in Table 1. It should be noted that the reverse Arrhenius parameters are fitted with a T^0 dependence in order to verify the accuracy of the thermochemical data. In

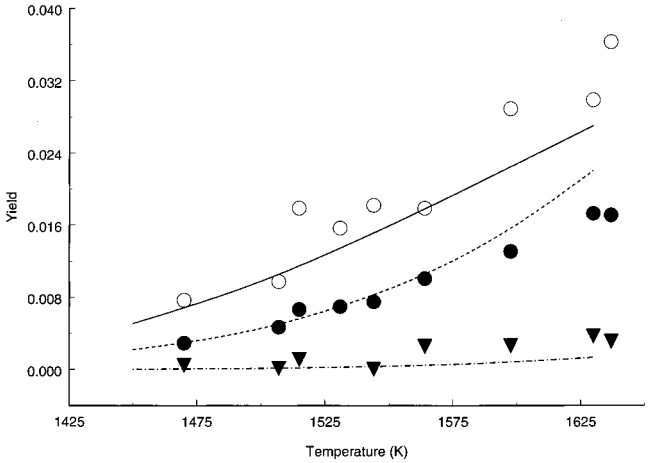

Figure 10. Variation with temperature of the experimental CO, CF_2O, and CO_2 yields. The respective experimental points are represented by the symbols (●, ○, ▼); model profiles are indicated by the lines: (—, - - -, - — -). Note that the CF_2O and CO_2 yields have been multiplied by 2 for clarity. Initial mixture: 6.2 mol % C_3F_6 and 0.6 mol % N_2O.

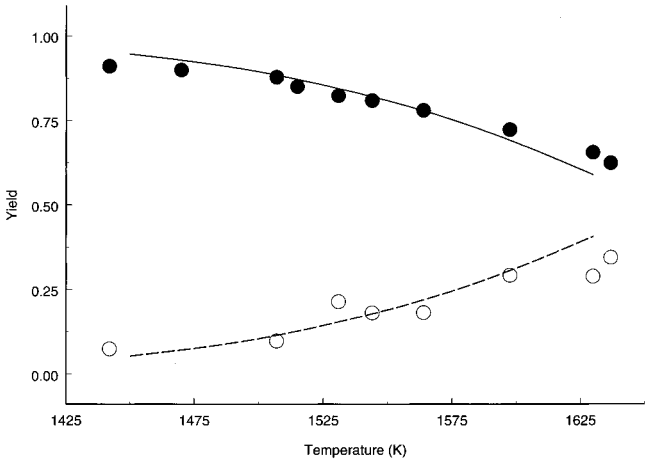

Figure 11. Variation with temperature of the experimental N_2O and N_2 yields. The respective experimental points are represented by the symbols (●, ○); model profiles are indicated by the lines: (—, - - -). Initial mixture: 6.2 mol % C_3F_6 and 0.6 mol % N_2O.

the actual numerical modeling, the reverse rate parameters are computed from the equilibrium constant at each temperature. The temperature dependences of the *A*-factors are included.

Many of the rate constants used for the fluorine chemistry were obtained from Burgess et al.[9] The nitrogen chemistry was obtained from Vandooren et al.[10] Some rate constants were obtained by fitting the known experimental data from a kinetic database.[11] Where these sources were insufficient, other references were used or estimates were made in this work.

The thermochemical data used in the modeling have been described in ref 2 except for that of CF_3CF, which has been modified in this work (vide infra).

Since it is the decomposition of N_2O that produces the $O(^3P)$ atoms, the kinetics of O atom formation are first discussed. The most important route for the destruction of N_2O is the unimolecular decomposition, $N_2O = N_2 + O$. The barrier of 265 kJ/mol and an *A*-factor of 2.7×10^{11} s^{-1} derived in this work yield a rate constant which, over the temperature range of 1000−2000 K, is in good agreement with current literature values.[11] It should be noted that under the experimental conditions (pressures ∼ 20 atm) this reaction should be at, or close to, the high-pressure limit. It is also a highly sensitive reaction, and the *A*-factor has thus been deduced with high precision.

The self-reaction, $N_2O + N_2O = N_2 + O + N_2O$, is also a sensitive reaction whose rate constant of $4 \times 10^{18}T^{-0.73}$ exp(−266 kJ mol^{-1}/RT) cm^3 mol^{-1} s^{-1} was obtained in this work. The *A*-factor obtained for this reaction agrees well with that of Vandooren et al.,[10] while the barrier is 3 kJ/mol higher than theirs. Also important is the reaction $N_2O + CO = CO_2 + N_2$. The *A*-factor of 8×10^{12} s^{-1} and the barrier of 151 kJ/mol were derived in this work. The resulting rate constant showed good agreement with the available literature values,[11] although the scatter in the literature is large.

There are only three reactions linking the fluorine and nitrogen chemistry in this mechanism. The first is the termolecular reaction of F atoms with NO forming FNO. For this reaction, the rate data used in the model are based on a fit of the available literature values; however, the data were measured at room temperature and therefore some uncertainty is associated with the rate constant. FNO was not detected in the second set of experiments, although the model does predict its presence. This may be attributed to its known high reactivity with metal surfaces.[12] The second reaction is $CF_3 + NO = CF_3NO$ whose rate constant is based on the room-temperature data of Masanet et al.[13] and uncertainties would also be expected with this rate constant. CF_3 can also react with FNO, yielding CF_4 and NO. The chosen rate constant is similar to that for the $CF_3 + ClNO$ reaction at 298 K.[14]

The most important reactions involving C_3F_6 are the addition of O atoms across the double bond. The addition is complicated by the possibility that O atoms can attack either carbon of the double bond; therefore, rate constants for attack at both these centers were included in the model. When the O atom adds to the terminal carbon, a triplet biradical is assumed to form, CF_3-$CF^{\bullet}CF_2O^{\bullet}$. This biradical is estimated to lie ∼130 kJ/mol below the energy of the reactants. This estimate is based on preliminary G2-MP2 calculations.[15] An error of at least 40 kJ/mol is assumed. The biradical can undergo three possible reactions. First, 1,2 F atom shift to form $CF_3CF_2 + CFO$ is possible. A barrier of 155 kJ/mol was estimated on the basis of the calculated barrier[15] for 1,2 F shift in the singlet $CF_3\ddot{C}F \rightarrow C_2F_4$ reaction. The products lie ∼60 kJ/mol below the biradical.

$$CF_3CF^{\bullet}CF_2O^{\bullet} \rightarrow CF_3CF_2 + CFO \qquad \Delta_rH = -60 \text{ kJ/mol}$$

Second, C−C rupture may occur to form the triplet $CF_3\ddot{C}F$ and CF_2O. These products also lie ∼60 kJ/mol below the energy of the biradical.

$$CF_3CF^{\bullet}CF_2O^{\bullet} \rightarrow {}^3CF_3\ddot{C}F + CF_2O \qquad \Delta_rH = -60 \text{ kJ/mol}$$

Third, F loss may occur to form $CF_3CF^{\bullet}CF{=}O$ + F (both doublets). The enthalpy of formation of $CF_3CF^{\bullet}CF{=}O$ ($\Delta_fH^\circ_{298}$ = −1045 kJ/mol) was estimated using the enthalpy of the aldehyde, $CF_3CF_2CF{=}O$ ($\Delta_fH^\circ_{298} = -1465$ kJ/mol; calculated by group additivities) and a C−F bond enthalpy of ∼500 kJ/mol. The products of this channel were estimated to lie ∼42 kJ/mol above the triplet biradical.

$$CF_3CF^{\bullet}CF_2O^{\bullet} \rightarrow CF_3CF^{\bullet}CF{=}O + F \qquad \Delta_rH = 42 \text{ kJ/mol}$$

A QRRK calculation[16] was performed considering all three channels. The high-pressure addition rate constant of 3.2×10^{12} cm^3 mol^{-1} s^{-1} was assumed, equivalent to that for O addition to C_2F_4 at 1500 K.[9] For the dissociation of the biradical back to reactants, an *A*-factor and barrier of 5.0×10^{13} s^{-1} and 130 kJ/mol were used. The *A*-factor and barrier for dissociation of

TABLE 1: Reaction Model for C_3F_6 Oxidation in N_2O[a]

	reaction	forward reaction log *A*	*n*	*E*	reverse reaction log *A*	*n*	*E*	ref; note
1	$2O + M = O_2 + M$	13.3	0	−7.5	14.7	0	488.6	33
2	$N_2O = O + N_2$	11.4	0	265.7	9.8	0	108.0	PW
3	$2N_2O = N_2 + O + N_2O$	18.6	−0.73	265.7	14.3	0	100.3	PW
4	$N_2O + O = 2NO$	13.8	0	107.2	12.2	0	265.5	10
5	$N_2O + O = N_2 + O_2$	13.9	0	114.5	13.6	0	453.7	11; fit
6	$NO + N = N_2 + O$	12.5	0.3	0.0	14.2	0	318.1	10
7	$NO + M = N + O + M$	15.1	0	621.0	14.4	0	−8.7	10
8	$NO + O = N + O_2$	9.6	1	173.1	13.8	0	51.1	10
9	$N + N_2O = N_2 + NO$	13.0	0	83.1	12.0	0	556.0	10
10	$NO_2 + O = NO + O_2$	12.6	0	−1.0	12.1	0	194.8	34
11	$NO_2 + M = NO + O + M$	15.3	0	292.9	12.4	0	−7.4	11; fit
12	$N_2O + CO = CO_2 + N_2$	12.9	0	150.6	13.6	0	516.8	PW
13	$2N + M = N_2 + M$	15.7	0	0.0	17.1	0	944.4	11; fit
14	$2NO + O_2 = 2NO_2$	9.1	0	4.4	11.5	0	108.9	35
15	$NO + N_2O = N_2 + NO_2$	14.4	0	209.2	14.6	0	352.6	11; fit
16	$2NO = N_2 + O_2$	13.2	0	254.8	14.5	0	435.8	11; fit
17	$O + CO + M = CO_2 + M$	19.0	−1.5	20.9	16.0	0	526.6	36
18	$O_2 + CO = O + CO_2$	12.4	0	200.0	13.4	0	227.0	33
19	$2F + M = F_2 + M$	10.1	0.77	117.2	11.7	0	−28.1	2
20	$F + NO + M = FNO + M$	16.2	0	2.5	17.4	0	229.7	11; fit
22	$CF_3 + NO = CF_3NO$	13.0	0	0.0	15.4	0	132.6	12
21	$CF_3 + FNO = CF_4 + NO$	11.5	0	0.0	13.5	0	307.2	13
23	$CF_3 + F = CF_4$	13.0	0	0.0	16.2	0	534.4	15
24	$CF_3 + F_2 = CF_4 + F$	12.4	0	10.5	14.4	0	390.7	37
25	$CF_3 + M = CF_2 + F + M$	16.0	0	348.9	14.2	0	−0.9	PW
26	$CF_3 + O_2 = CF_3O + O$	9.4	1.14	90.0	13.6	0	5.5	9
27	$CF_3 + O = CF_2O + F$	13.0	0	0.0	13.6	0	303.2	38; *A*/2
28	$CF_2O + F = CF_3O$	12.4	0	33.9	13.3	0	129.1	39
29	$CF_3O + F = CF_3OF$	13.0	0	0.0	14.5	0	206.7	40; *A*/3
30	$CF_2 + O_2 = CF_2O + O$	13.3	0	110.9	14.3	0	267.8	25
31	$CF_3CF + O_2 = CF_3COF + O$	13.3	0	110.9	14.0	0	370.6	estd
32	$CF_2 + O = CFO + F$	13.6	0	4.2	13.4	0	160.1	9; *A*/2
33	$CF_3CF + O = CFO + CF_3$	13.0	0	0.0	12.1	0	381.8	PW
34	$CF_3CF + F = CF_2 + CF_3$	13.0	0	4.2	12.3	0	230.1	PW
35	$CF_3CF = CF_3 + CF$	15.0	0	288.7	12.5	0	14.7	PW
36	$CF + F = CF_2$	13.8	0	0.0	15.6	0	500.0	9
37	$CF + O_2 = CFO + O$	13.3	0	7.5	13.5	0	167.3	9
38	$CF + O = CO + F$	13.9	0	4.2	15.0	0	527.4	9; A*2
39	$F + CFO = F_2 + CO$	11.1	0	33.5	11.7	0	55.1	9
40	$CFO + F = CF_2O$	12.0	0	0.0	14.6	0	497.2	PW
41	$CFO + F_2 = CF_2O + F$	12.8	0	13.4	14.3	0	356.3	11; fit
42	$CFO = CO + F$	25.0	−4.46	141.0	8.5	0	−43.5	PW
43	$CFO + O = CO_2 + F$	13.9	0	0.0	15.8	0	390.5	9; 3*A*
44	$2CFO = CO + CF_2O$	13.3	0	1.3	15.4	0	365.9	41
45	$2CF_3 = CF_3{-}CF_3$	13.5	0	0.0	17.3	0	381.8	42
46	$CF_3{-}CF_2 + O \rightarrow CF_3 + CFO + F$	13.3	0	0.0			0.0	9
47	$CF_3{-}CF_2 + O = CF_2O + CF_3$	13.0	0	0.0	13.1	0	438.5	9
48	$CF_3{-}CF_2 = CF_3 + CF_2$	15.6	0	235.4	13.3	0	20.9	43
49	$CF_3{-}CF_2 + F = 2CF_3$	13.5	0	0.0	12.9	0	135.3	44; C_2H_5+H
50	$CF_2CF_2 = 2CF_2$	16.7	0	292.6	13.5	0	30.5	45
51	$CF_3CF = CF_2CF_2$	12.2	0	150.6	13.0	0	288.9	14
52	$CF_2CF_2 + O = CF_2 + CF_2O$	9.3	1	0.0	12.0	0	402.6	9
53	$CF_2CF + O_2 = CF_2O + CFO$	26.7	−4.55	22.9	10.9	0	532.5	9
54	$CF_2CF + O = CF_2CO + F$	13.5	0	0.0	14.3	0	246.0	9
55	$2CF = C_2F_2$	13.7	0	0.0	17.3	0	441.7	estd
56	$C_2F_2 + O = CFCO + F$	7.0	2	7.9	12.8	0	155.6	9
57	$CF_2CF = C_2F_2 + F$	13.3	0	334.7	13.1	0	26.2	estd
58	$CF_2CO + O = CF_2O + CO$	13.0	0	33.5	13.6	0	713.5	9
59	$CFCO + O = CFO + CO$	14.0	0	0.0	14.5	0	613.0	9
60	$CFCO + F = CF_2 + CO$	13.5	0	0.0	14.2	0	457.2	9; *A*/3
61	$CF_2CF_2 + F = CF_3 + CF_2$	13.8	0	0.0	12.3	0	87.7	9; 2*A*
62	$CF_2CF_2 + F = CF_3{-}CF_2$	13.8	0	32.5	14.7	0	334.7	2
63	$CF_2CF + F = 2CF_2$	13.3	0	0.0	13.2	0	249.7	9
64	cyclo-$C_3F_6 \rightarrow CF_2CF_2 + CF_2$	13.0	0	182.0			0.0	2
65	$CF_2CF_2 + CF_2 \rightarrow$ cyclo-C_3F_6	11.5	0.5	35.6			0.0	2
66	$2CF_3CF = 2\text{-}C_4F_8$	11.7	0	12.6	14.2	0	550.9	2; *A*/10
67	$2CF_2CF = C_4F_6$	12.5	0	0.0	17.5	0	551.5	2
68	$C_3F_6 + CF_2 = i\text{-}C_4F_8$	12.0	0	133.9	15.9	0	402.2	2; *A*/40
69	$C_3F_6 + F = CF_3{-}CF_2 + CF_2$	13.4	0	0.0	12.8	0	44.7	PW
70	$C_3F_6 + F = CF_3CF + CF_3$	13.5	0	50.2	13.0	0	4.3	PW
71	$C_3F_6 + O = CF_3CF + CF_2O$	12.7	0.05	0.4	12.7	0	257.6	PW;QRRK fit
72	$C_3F_6 + O \rightarrow CF_3 + CF_2CF{=}O$	12.5	0	0.0	0.0	0	0.0	PW
73	$CF_2CF{=}O \rightarrow CFO + CF_2$	15.3	0	250.0				
74	$C_3F_6 = CF_3 + CF_2CF$	16.7	0	441.8	13.9	0	22.4	PW
75	$C_3F_6 = CF_3CF + CF_2$	15.7	0	401.7	13.4	0	6.0	PW
76	$CF_3{-}CF_2 + CF_2 = n\text{-}C_3F_7$	12.6	0	8.4	14.8	0	205.6	2
77	$n\text{-}C_3F_7 = CF_2CF_2 + CF_3$	14.7	0	190.0	13.3	0	40.4	2; 5*A*
78	$CF_3O + CO = CO_2 + CF_3$	10.5	0	0.0	11.4	0	124.7	estd

[a] Units for *A*, $cm^3\ mol^{-1}\ s^{-1}$ or s^{-1} as appropriate. Units for *E*, kJ/mol. PW indicates rate constant evaluated in the present work. Estd. indicates rate constant was estimated in the present work; fit indicates that the database of ref 11 was used to provide a fit to currently known rate data; 2*A* and *A*/2 indicates *A*-factor multiplied and divided by 2 for this work. The carbene CF_3CF produced in reaction 71 is assumed to be initially a triplet, but at ~20 atm, rapid spin relaxation to the singlet state is expected to occur (see text).

the biradical via the first channel are $1.6 \times 10^{12}\ s^{-1}$ and 155 kJ/mol; the parameters for the second channel were $2.0 \times 10^{15}\ s^{-1}$ and 13 kJ/mol. The parameters for the third channel were $A = 2 \times 10^{14}\ s^{-1}$ and 55 kJ/mol (reaction endothermicity plus a 13 kJ/mol barrier). The calculation showed that the second channel, with its negligible barrier, proceeds with a rate that is several orders of magnitude faster than the first channel and at least a factor of 100 faster than the third channel. Therefore, the overall rate constant for O-addition to form triplet $CF_3\ddot{C}F$ and CF_2O is $3.2 \times 10^{12}\ cm^3\ mol^{-1}\ s^{-1}$ at 1500 K (note that the QRRK fit is used as the rate constant for reaction 71 in Table 1).

Under the high-pressure conditions of these experiments, it is assumed that the triplet $CF_3\dot{C}F$ will undergo rapid collision-induced spin relaxation to form the singlet carbene. This assumption is justified in part by the quenching rate constant[17] of $^3CF_2$ by O_2 of 2.5×10^{12} cm^3 mol^{-1} s^{-1}. The $^3CF_2$ quenching experiments of Young et al.[18] show that NO and O_2 are significantly better quenchers than Ar. The predicted concentrations of NO in the first and third sets of experiments in this paper are $\sim 1 \times 10^{-9}$ mol cm^{-3}; in the second set, [NO] $\approx 1 \times 10^{-6}$ mol cm^{-3}. The quenching rate constant determined by Koda[19] for $^3CF_2$ and NO of 2.9×10^{13} cm^3 mol^{-1} s^{-1} gives a lifetime of ~ 25 μs for sets I and III; for set II, the lifetime is only 0.03 μs. Another indication is given by the rate constant for triplet SO_2 relaxation[20] with argon as the collider species. The rate constant for $^3SO_2$ spin relaxation is 3.3×10^{10} cm^3 mol^{-1} s^{-1}, and this gives the triplet state lifetime of 0.2 μs at 20 atm and 1500 K.

Although the rate constant for $^3CF_3\dot{C}F$ is not known, the studies on $^3CF_2$ and $^3SO_2$ suggest that the upper-limit lifetime of $^3CF_3\dot{C}F$ should be fractions of microseconds. The shock-tube experiments of this work have reaction times of hundreds of microseconds. Second, NO, O_2, and Ar are present in the reaction mixture, and these should adequately quench the $^3CF_3C\ddot{F}$. Therefore, the $^3CF_3\dot{C}F$ should not contribute significantly to the overall chemistry of the system.

The singlet−triplet energy gap for the $CF_3\dot{C}F$ has been determined in recent difference-dedicated configuration interaction calculations by Garcia et al.[21] and CBS-Q calculations by van Stekelenborg.[22] A value of 72 kJ/mol was found, with the singlet being lower in energy. This energy gap further suggests that rapid triplet−singlet conversion should occur, especially when the singlet is thermodynamically more stable.

When O-addition to the central carbon occurs, it is suggested that the triplet biradical $CF_2{}^{\bullet}CFO{}^{\bullet}CF_3$ forms. Its energy is assumed to lie $\sim$130 kJ/mol below the reactants. This triplet biradical can undergo C−C bond scission to form CF_3 and $^{\bullet}CF_2$-CF=O radicals (both doublets). The latter radical has an estimated $\Delta_f H°_{298} = -613$ kJ/mol based on the enthalpy of formation of $CF_3CF{=}O$ ($\Delta_f H°_{298} = -1024$ kJ/mol; calculated by isodesmic reactions at the G2-MP2 level[15]) and a C−F bond enthalpy of $\sim$500 kJ/mol. The energy of the products lies 75 kJ/mol below that of the triplet biradical; the rupture should be rapid because of the high *A*-factor ($\sim 10^{15}$ s^{-1}) and large exothermicity.

$$CF_2{}^{\bullet}CFO{}^{\bullet}CF_3 \rightarrow {}^{\bullet}CF_2CFO + CF_3 \qquad \Delta_r H = -75 \text{ kJ/mol}$$

This biradical could also undergo C−C scission to form the triplet CF_2 and singlet CF_3CFO. To determine the energy of the products, the enthalpy of formation of the triplet CF_2 (47.4 kJ/mol) was required. This enthalpy was deduced by adding the calculated singlet−triplet energy gap (234 kJ/mol [17]) to the enthalpy of formation of the singlet (−186.6 kJ/mol[9]). The energy of the products was found to lie $\sim$90 kJ/mol above that of the $CF_3 + {}^{\bullet}CF_2CF{=}O$.

$$CF_2{}^{\bullet}CFO{}^{\bullet}CF_3 \rightarrow CF_3CF{=}O + {}^3CF_2 \qquad \Delta_r H = 19 \text{ kJ/mol}$$

A third possible channel is the elimination of F atoms from the triplet biradical to form $CF_3C{=}OCF_2{}^{\bullet}$ (estimated $\Delta_f H°_{298} = -975$ kJ/mol based on $\Delta_f H°_{298} = -1398$ kJ/mol for $CF_3C{=}OCF_3$[23] and a C−F bond enthalpy of $\sim$500 kJ/mol). The reaction is endothermic and lies $\sim$185 kJ/mol above that of the $CF_3 + {}^{\bullet}CF_2CF{=}O$.

$$CF_2{}^{\bullet}CFO{}^{\bullet}CF_3 \rightarrow CF_3CF{=}OCF_2{}^{\bullet} + F \qquad \Delta_r H = 110 \text{ kJ/mol}$$

Because of the endothermicity of these last two channels, it is assumed that only the first channel is important.

The most likely fate of the $^{\bullet}CF_2CFO$ radicals is C−C rupture to form singlet CF_2 and CFO radicals. Although the bond enthalpy is $\sim$250 kJ/mol, the high *A*-factor ($\sim 10^{15}$ s^{-1}) would ensure that this is a rapid process.

$$^{\bullet}CF_2CFO \rightarrow {}^1\ddot{C}F_2 + CFO \qquad \Delta_r H = 250 \text{ kJ/mol}$$

In the kinetic model, the O-addition to the central carbon is treated as a two-step process. The reaction is assumed to rapidly form $^{\bullet}CF_2CFO + CF_3$, with a rate constant of 3.2×10^{12} cm^3 mol^{-1} s^{-1}. The second step is the irreversible decomposition of the $^{\bullet}CF_2CFO$ radicals to $^1\ddot{C}F_2 + CFO$. The *A*-factor is assumed to be 2×10^{15} s^{-1} with a barrier of 250 kJ/mol.

Both of the above additions could also proceed along singlet surfaces to form a stable epoxide, C_3F_6O, where the addition reaction would have to proceed over a barrier associated with triplet−singlet curve-crossing. However, epoxides were not detected in any of the experiments, further indicating that both reactions probably follow triplet surfaces.

When O atoms add to the central carbon of C_3F_6, traces of CF_3CFO were observed in the room-temperature experiments of Saunders and Heicklen.[3] Because the formation of CF_3CFO and $^3CF_2$ from the triplet biradical is endothermic by 19 kJ/mol the CF_3CFO could only form by way of a triplet to singlet curve-crossing. As their experiments involved photosensitization by the heavy atom Hg*, it is possible that triplet−singlet crossing could take place via spin−orbit perturbations through a short-lived complex incorporating the Hg.

The pyrolysis reactions for C_3F_6 were important in the modeling of the third reaction set (excess C_3F_6). The *A*-factors for both the unimolecular single- and double-bond rupture were optimized to give the correct product distributions (residual C_3F_6 and C_2F_4). Rupture of the double bond leads to the singlet carbenes $CF_3C\ddot{F}$ and CF_2. In previous work, the enthalpy of formation for $CF_3\dot{C}F$ at 298 K was estimated by Hynes et al.[2] to be −586 kJ/mol. However, recent G2-MP2 isodesmic reaction calculations[15] now give the heat of formation at 298 K to be −520 kJ/mol. This value is in excellent agreement with a value of −523 kJ/mol computed at the CBS-Q level by van Stekelenborg.[22] The ab initio barrier and *A*-factor for the isomerization[15] of the carbene into C_2F_4 result in a higher *A* value and a lower activation energy compared with that found in previous work.[2] These ab initio values are incorporated into the modeling in this work.

The addition of F atoms to C_3F_6 was also complicated by the possibility of addition to either carbon of the double bond, and two reactions were included to describe these. Rate constants for both of these reactions were estimated based on the $C_2F_4 +$ F rate constant of Burgess et al.[9]

Other important secondary reactions include reactions of F atoms with radicals and other molecules. These include the termination of CF_3 with F forming CF_4, a product that is only detected in runs where ignition has occurred. The bimolecular rate constant of Plumb and Ryan[24] measured at 298 K was used. At $\sim$20 atm, this reaction is likely to be close to the high-pressure limit. The rate constant for the reaction of CF_2 and O yielding CFO and F is based on that of Burgess et al.,[9] with the

A-factor reduced by a factor of 2 in this work. The rate constant for the reaction of $CF_3\ddot{C}F$ and O was estimated on the basis of the aforementioned reaction except that the barrier is assumed to be negligible and the *A*-factor slightly lower. In this work, it is assumed that the reactants singlet $CF_3\ddot{C}F$ and $O(^3P)$ correlate with the products CFO and CF_3 on a triplet surface, rather than with CF_3CFO on a singlet surface (which would include a barrier for association and curve-crossing). The rate constant estimated for $O_2 + CF_3\ddot{C}F$ is assumed to be equal to that derived by Keating and Matula[25] for CF_2 and O_2.

A sensitive reaction in this study is the unimolecular decomposition of the FCO radical. Under the high-pressure conditions of this work (~20 atm), the termolecular association rate constant F + CO + M = FCO + M derived by Burgess et al.[9] (at 1 atm) was found to be inappropriate under our experimental conditions. Therefore, an RRKM calculation was performed for the unimolecular decomposition, FCO = F + CO, with the UNIMOL[26] program using the transition state geometry of Francisco[27] calculated at the MP2 level and the critical energies of Knyazev et al.[28] The value of $\langle \Delta E \rangle_{down} = 350\ cm^{-1}$ was used in the calculation. At 20 atm, a rate constant for the unimolecular decomposition reaction of $10^{25.8}T^{-4.46}$ exp(−141 kJ mol^{-1}/*RT*) was derived; however, the *A*-factor was reduced by a factor of 5 to ensure correct modeling of the products. This RRKM calculation for the FCO decomposition showed good agreement with the 1 atm value of Burgess et al.[9] (the reverse rate constant is calculated from the equilibrium constant at 1500 K) and the correct falloff behavior was predicted when compared with the low-pressure experimental results of Knyazev et al.[28] However, the high-pressure limit for the FCO decomposition was not reached at 1000 atm where the calculated $k_{uni}/k_\infty \cong 8 \times 10^{-2}$ at 1500 K. This suggests that the rate constant used in this work is reasonable in light of the uncertainties in the RRKM calculations and the absence of a measured high-pressure limit value for the decomposition.

Kinetic Modeling. Kinetic modeling with the mechanism given in Table 1 was performed with the Sandia code CHEMKIN[29] together with a shock-tube code[30] modified to include the effects of quenching by the reflected rarefaction wave and the LSODE ordinary differential equation solver.[31] The code SENKIN[32] was used for sensitivity analyses.

Figures 1−3 show the results of modeling the first set of experimental data. These figures show that all major stable product and unconsumed reactant yields have been modeled successfully over the temperature range.

Figures 6−9 show the results of modeling the second data set in which ignition takes place. In Figure 6, the model tends to overpredict the rate of C_3F_6 consumption somewhat. The peak C_2F_6 yield is predicted to be ~40% higher than that observed experimentally; however, this could also be attributed to difficulties in obtaining experimental yield data at the precise temperature where ignition occurs. The C_2F_4 yield is also slightly overpredicted by the model. Figure 7 shows that the model reproduces the 'spike' in the CO profile, and the CO_2 and CF_2O profiles have also been successfully modeled. Figure 8 shows that good agreement was obtained between model and experimental CF_4 and O_2 yield profiles.

As stated above, small yields of NO and NO_2 were detected in the products, the latter products possibly arising from NO oxidation by O_2 in the infrared cell. The kinetic model predicts that NO_2 should be essentially undetectable under these shock conditions, further supporting the view that the measured NO_2 is indeed an artifact.

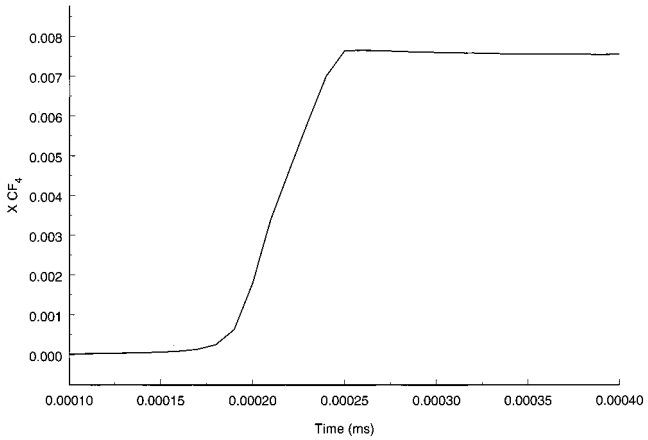

Figure 12. Plot of CF_4 model mole fractions (—) versus time for an experiment which exhibits ignition. The initial temperature was 1540 K. Initial mixture: 0.7 mol % C_3F_6 and 6.3 mol % N_2O.

The ignition delay mentioned above has been simulated using the chemical kinetic model. To achieve this, the model CF_4 mole fraction was calculated with a constant-pressure model and plotted against time as shown in Figure 12. This species was chosen because it is present in significant quantities only after ignition. The time required for the CF_4 to reach 50% of its equilibrium mole fraction is about 220 μs. This delay time is in good agreement with the observed ignition delay time of 240 ± 50 μs. Note that a constant volume calculation predicts a delay time that is 50 μs shorter.

Figures 9−11 show that the model has provided good fits to all the major species for the third set of experimental data. The two isomers of C_4F_8 were also detected in low yields in the experiments. Although these species were accounted for in the kinetic model, their yields are too small to model accurately and their yield profiles were thus omitted in this work.

Sensitivity and Rate of Production Analyses. Reaction flux analyses for all sets were performed at a short reaction time of 100 μs to avoid thermal equilibration. Also, the calculated temperature, assuming a constant-pressure system, increases rapidly after 100 μs in the set II analyses due to ignition and decreases in set III due to reaction cooling behind the reflected shock front.

Set I. In terms of the rate of production of O atoms, the reaction with the most flux is reaction 3, the N_2O self-reaction, which accounts for 100% O atom production. O atom addition to both the terminal and central carbons of the double bond (reactions 71 and 72, respectively) is important in the destruction of the C_3F_6. As the temperature rises from 1390 to 1495 K, the addition of F atoms to the central carbon (reaction 69) becomes the dominant C_3F_6 destruction route with 40% of the flux. The addition of O atoms to either of the double-bonded carbons of C_3F_6 plays a lesser role (30% by reaction 71, 15% by reaction 72). F atoms are produced predominantly by reaction 42 (CFO = CO + F; 33%) and reaction 32 ($CF_2 + O = CFO + F$; 16%). The major consumption route of F atoms is reaction 69. FCO is an important radical in this system and is generated by reaction 73 (26%) and by reaction 32 (23%); reaction 42 is the primary consumption channel. An interesting feature of the rate of production analysis is that a radical chain mechanism operates, enabling F-atom attack to proceed more efficiently than O-atom attack. The F atoms produced by reactions 42 and 32 are consumed in the F attack on C_3F_6 (reaction 69). The resulting fluoroethyl radicals undergo C−C rupture producing CF_3 (the primary production route for this radical) and CF_2. The CF_2 produced by this reaction and reaction 50 (C_2F_4 pyrolysis) is

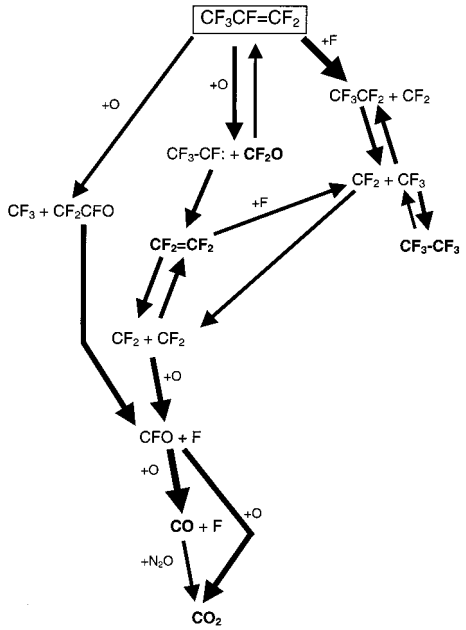

Figure 13. Reaction fluxes for C_3F_6 decomposition and product formation. The largest arrows indicate the channels with the greatest flux. The conditions are 1.5% N_2O and 0.6% C_3F_6 at a temperature of 1500 K.

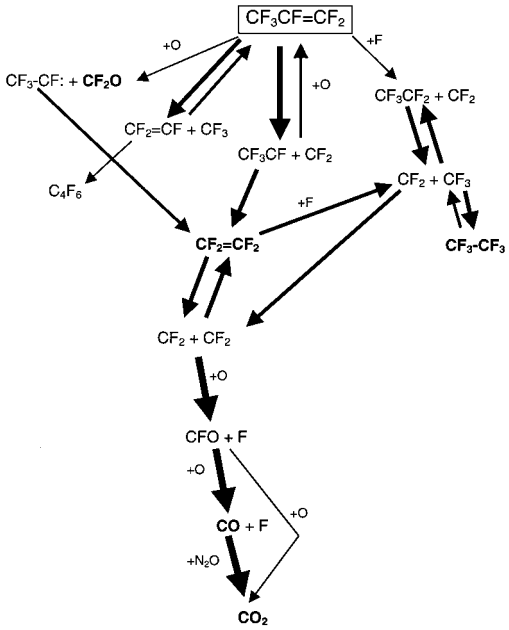

Figure 14. Reaction fluxes for C_3F_6 decomposition and product formation. The largest arrows indicate the channels with the greatest flux. The conditions are 0.6% N_2O and 6.3% C_3F_6 at a temperature of 1600 K.

successively oxidized by O atoms to CFO and then CO, with F production accompanying each reaction. The F so produced reacts with C_3F_6 to continue the chain.

The formation and destruction channels of the important stable products are shown schematically in Figure 13. CF_2O, under these conditions, is particularly stable and has no significant decomposition channel.

The sensitive reactions involving C_3F_6 are the O-atom addition reactions 71 and 72. Also important is the $CF_2 + O$ reaction 32. The most sensitive reaction for all products is N_2O decomposition (reaction 2). Also sensitive are reactions 12, 32, and 43.

Set II. At temperatures below the point of ignition (~1450 K), the oxidation proceeds as described in set I. An analysis of the flux data at 1550 K shows that decomposition of C_3F_6 becomes driven by F addition reaction (reaction 69). This is a result of significantly greater flux through reactions 32 and 42. The formation pathways for CF_2O have also changed with reaction 71 decreasing in flux and reaction 44 (CFO recombination; 42%) becoming dominant. Reaction 27 ($O + CF_3$) accounts for 20% of CF_2O formation. In terms of CO and CO_2 production, the pathways are similar to those described in the previous set except that greater flux passes through reaction 12 in the case of CO_2 formation. C_2F_6 and C_2F_4 formation routes are as described in Figure 13.

Two species observed in set II and not observed in set I are CF_4 and O_2. The formation of the former was through reaction 23 (99%), although the consumption of F by this channel was 6% and CF_3 consumption was less than 1%. O_2 formation was caused by reaction 5 where N_2O consumes O.

Reaction rate sensitivities and fluxes are also used to explain the basis of the ignition process. Sensitivities for this set are studied at an initial temperature of 1550 K and 20 atm. At short reaction times, the oxidation of C_3F_6 is dominated by O-addition reactions 71 and 72. From reactions 32 and 73 CFO is produced. This subsequently breaks down to F and CO (reaction 42). At longer times, the F attacks the C_3F_6 through reaction 69 producing CF_2 radicals. F also attacks C_2F_4 producing CF_2 and CF_3 (reaction 61). The CF_2 reacts with O atoms (reaction 32) to produce F and CFO. In this way, a high concentration of F atoms build up, propagated by reactions 61 and 69. The F atom attack reactions are all exothermic as written ($\Delta_r H = -46$ and -80 kJ/mol for reactions 69 and 61, respectively) and the O atom reactions are even more exothermic ($\Delta_r H = -160$, -255, and -203 kJ/mol for reactions 32, 71, and 72, respectively). Ignition in this set occurs due to the large concentration of O atoms and the large flux through reactions 71 and 72. Reactions 32 and 42 also have a greater flux than in set I. This creates a pool of F atoms that are consumed through reactions 69 and 61. The constant pressure sensitivity calculations show an increase in temperature of ~250 K at the end of the reaction time.

Set III. Analysis of this set shows the expected pyrolytic behavior since a large excess of C_3F_6 was used. The dominant C_3F_6 decomposition pathways were reactions 75 (double bond rupture) and 74 (single bond rupture). Reaction 75 dominated over 74 as a result of its lower barrier. The flux through the O-addition channels is less than in the previous reaction sets with only 3% consumption of C_3F_6 taking place at 1600 K through reaction 71. Reactions 75 and 71 produce the carbene $CF_3\dot{C}F$ and reaction 74 produces the fluorovinyl radical $CF_2{=}\dot{C}F$. The primary decomposition routes for CF_3CF are reactions -75 and the 1,2 F-shift isomerization reaction, 51, producing C_2F_4. Reaction -74, producing C_3F_6, and the recombination into C_4F_6 consume the fluorovinyl radicals (reaction 67).

Since the O atom is in lower concentrations in this set, less CFO is produced and hence less F. The F attack on C_3F_6 (reaction 69) is less important in this series and consumes only 6.5% of the C_3F_6 at 1600 K. Reactions producing F and CFO are as described in the previous two sets. The flux diagram in Figure 14 shows the production and consumption routes of the major products. The formation and destruction of C_2F_6 and C_2F_4 are as described in sets I and II. CF_2O is essentially formed by reaction 71, CO entirely by reaction 42, and CO_2 by reactions 12 (94%) and 43 (6%).

At 1600 K and low residence times, the C_3F_6 mole fraction displays sensitivity to reactions 75, 51, 68, and 67. Significantly,

reaction 75 has greater sensitivity than reaction 2. The C_2F_4 also displays sensitivity to reactions 75 and 51. The remaining products are sensitive to reactions already described in the previous two sets.

Role of C_3F_6 in C_3 Fluorocarbon Flame Inhibition. In the context of flame inhibition by CF_3CHFCF_3, C_3F_6 can play an important role. In lean, atmospheric pressure flames,[1] the thermal decomposition route forming C_3F_6 accounts for ~40% of the calculated CF_3CHFCF_3 decomposition channels. In these lean, atmospheric pressure flames, C_3F_6 could not be detected in the postflame gases. Because flame radicals such as H, O, and OH are in superequilibrium concentrations in the reaction zone of the flame, rapid exothermic destruction of the C_3F_6 is expected on the basis of the results of this work. The ignition behavior of C_3F_6 as described in set II could, in part, account for the large temperature increases observed when CF_3CHFCF_3 is added to a flame. The ignition process however depends on the relative O and C_3F_6 concentrations. A near-stoichiometric mixture did not ignite, but a 10-fold excess of O atoms did cause ignition.

Despite a lack of knowledge of certain rate data for C_3F_6 destruction in a flame, especially channels involving OH, our reaction flux analysis of the CF_3CHFCF_3-inhibited flame data[1] suggests that OH addition to C_3F_6 would still be the dominant destruction route, although O + C_3F_6 reactions are nonetheless important channels. Because inhibitor molecules such as CF_3CHFCF_3 decompose exothermically in a flame, the extra heat released through C_3F_6 ignition (if the C_3F_6 were in an O-atom-rich environment) could lead to increased flame propagation, rather than inhibition. This may contribute to the relative inefficiency of CF_3CHFCF_3 as an inhibitor compared with CF_3Br.

The behaviors of perfluoroalkenes and perfluoroalkanes are markedly different. As shown in this paper, the initiation step for the oxidation of C_3F_6 is essentially a barrierless process. In contrast, the routes for perfluoroalkane (e.g., C_2F_6) decomposition are C−C scission (barrier ~406 kJ/mol), C−F loss (515 kJ/mol), and F abstraction by O (300 kJ/mol). Because of these high-energy destruction routes, perfluorinated alkanes tend to behave thermally (via heat absorption and dilution) rather than chemically in a flame environment. Perfluoroalkenes tend be more fuel-like.[4]

Conclusion

An examination of the product yields and reaction path analysis of the reaction between C_3F_6 and N_2O shows that C_3F_6 decomposes primarily by O addition to both carbons of the double bond. The analysis also shows that, when CFO radicals form, they readily undergo unimolecular F loss. These F atoms are then able to attack the C_3F_6 and cause a radical chain that also involves CF_2 carbenes. Significantly, no CF_3CFO or the epoxide, C_3F_6O, was observed in any of the experiments, suggesting that O-addition proceeds along a triplet surface. In the presence of excess N_2O, ignition was observed to occur at temperatures above ~1410 K, owing to the large excess of O atoms and the resulting large F radical production. The reactions that give rise to ignition are initiated by O addition to both carbons of the double bond, reactions 71 and 72. The flux through these two reactions is greater than in set I owing to the large excess of O atoms. The subsequent exothermic oxidation of CF_2 (reaction 32) and unimolecular decomposition of CFO radicals (reaction 42) produce F atoms. The large pool of F atoms so produced reacts with C_3F_6 and C_2F_4 via reactions 61 and 69 respectively producing CF_2 and CF_3 radicals, ultimately. The large F pool is evidenced by the observation of CF_4, which forms from the recombination of F and CF_3 radicals. Despite the large concentration of O atoms in set II, partial, rather than complete, oxidation takes place, with CF_2O and CO being the major partially oxidized products. The rate constant for O_2 oxidation of CO (reaction 18) has a high (200 kJ/mol) barrier, and the O_2 concentration is relatively low except under the conditions of high temperatures and large O excess. The rate constant for O atom oxidation of CO (reaction 17) is termolecular and therefore slow. The dominant route for CO oxidation to CO_2 is by N_2O oxidation (reaction 12) by virtue of the large N_2O concentrations used.

Under C_3F_6-rich conditions, pyrolysis was observed with the rupture of both single and double bonds being the principal decomposition reactions.

Acknowledgment. We thank Dr. G. B. Bacskay and Mr. M. Smith for performing G2-MP2 calculations.

References and Notes

(1) Hynes, R. G.; Mackie, J. C.; Masri, A. R. *Combust. Flame* **1998**, *113*, 554.
(2) Hynes, R. G.; Mackie, J. C.; Masri, A. R. *J. Phys. Chem. A* **1999**, *103*, 54.
(3) Saunders, D.; Heicklen, J. *J. Am. Chem. Soc.* **1965**, *87*, 4062.
(4) Douglass, C. H.; Ladouceur, H. D.; Shamamian, V. A.; McDonald, J. R. *Combust. Flame* **1995**, *100*, 529.
(5) Bauer, S. H.; Hou, K. C.; Resler, E. L., Jr. *Phys. Fluids Suppl.* **1969**, *1*, 125.
(6) Shurvell, H. F.; Dass, S. C.; Gordon, R. D. *Can. J. Chem.* **1974**, *52*, 3150.
(7) Lagemann, R. T.; Jones, E. A.; Woltz, P. J. H. *J. Chem. Phys.* **1952**, *20*, 1768.
(8) Chen, J.; Zhu, T.; Niki, H. *J. Phys. Chem.* **1992**, *92*, 6115.
(9) Burgess, D. R., Jr.; Zachariah, M. R.; Tsang, W.; Westmoreland, P. R. *Prog. Energy Combust. Sci.* **1996**, *21*, 453.
(10) Vandooren, J.; Van Tiggelen, P. J.; Pauwels, J.-F. *Combust. Flame* **1997**, *109*, 647.
(11) Westley, F.; Herron, J. T.; Frizzell, D.; Hampson, R. F.; Mallard, W. G. *NIST Chemical Kinetics Database 17−2Q98*; NIST Standard Reference Data; NIST: Gaithersburg, MD, 1998.
(12) Greenwood, N. N.; Earnshaw, A. *Chemistry of the Elements*; Pergamon Press: Oxford, U.K., 1993; p 507.
(13) Masanet, J.; Caralp, F.; Ley, L.; Lesclaux, R. *Chem. Phys.* **1992**, *160*, 383.
(14) Rossi, M. J.; Barker, J. R.; Golden, D. M. *J. Chem. Phys.* **1979**, *71*, 3722.
(15) Smith, M. B. Sc. (Hons) Thesis, School of Chemistry, University of Sydney, 1998.
(16) Dean, A. M.; Westmoreland, P. R. *Int. J. Chem. Kinet.* **1987**, *19*, 207.
(17) Koda, S. *Chem. Phys.* **1982**, *66*, 383.
(18) Young, R. A.; Blauer, J.; Bower, R.; Lin, C. L. *J. Chem. Phys.* **1988**, *88*, 4834.
(19) Koda, S. *J. Phys. Chem.* **1979**, *83*, 2065.
(20) Briggs, J. P.; Caton, R. B.; Smith, M. J. *Can. J. Chem.* **1975**, *53*, 2133.
(21) Garcia, V. M.; Castell, O.; Reguero, M.; Caballol, R. *Mol. Phys.* **1996**, *87*, 1395.
(22) Van Stekelenborg, J. Private communication, January 1999.
(23) Gordon, A. S. *Int. J. Chem. Kinet.* **1972**, *4*, 541.
(24) Plumb, I. C.; Ryan, K. R. *Plasma Chem. Plasma Process.* **1986**, *6*, 11.
(25) Keating, E. L.; Matula, R. A. *J. Chem. Phys.* **1977**, *66*, 1237.
(26) Gilbert, R. G.; Smith, S. C.; Jordan, M. J. T. *UNIMOL Program Suite for the Calculation of Falloff Curves for Unimolecular and Recombination Reactions*; School of Chemistry, University of Sydney: Sydney, 1993.
(27) Francisco, J. S.; Goldstein, A. N.; Williams, I. H. *J. Chem. Phys.* **1988**, *89*, 3044.
(28) Knyazev, V. D.; Bencsura, A.; Slagle, I. R. *J. Phys. Chem.* **1989**, *93*, 1916.
(29) Kee, R. J.; Miller, J. A.; Jefferson, T. H. *CHEMKIN, A General Purpose, Problem Independent, Transportable FORTRAN Chemical Kinetics Code Package*; Report SAN80-003; Sandia Laboratories: Albuquerque, NM, March 1980.

(30) Mitchell, R. E.; Kee, R. J. *A General Purpose Computer Code for Predicting Chemical Kinetic Behavior Behind Incident and Reflected Shocks*; Report SAN82-8205; Sandia Laboratories: Albuquerque, NM, March 1982.
(31) Hindmarsh, A. C. *LSODE and LSODI, Two New Initial Value Differential Equation Solvers*; ACM Signum Newsletter **1980**, *15*, 4.
(32) Lutz, A. E.; Kee, R. J.; Miller, J. A. *SENKIN: A FORTRAN Program Predicting Homogeneous Gas-Phase Chemical Kinetics with Sensitivity Analysis*; Report SAND87-8248: Sandia Laboratories: Albuquerque, NM, Feb 1988.
(33) Tsang, W.; Hampson, R. F., Jr. *J. Phys. Chem. Ref. Data* **1986**, *15*, 1087.
(34) Tsang, W.; Herron, J. T. *J. Phys. Chem. Ref. Data* **1991**, *20*, 609.
(35) Atkinson, R.; Baulch, D. L.; Cox, R. A.; Hampson, R. F., Jr.; Kerr, J. A.; Rossi, M. J.; Troe, J. *J. Phys. Chem. Ref. Data* **1997**, *26*, 1329.
(36) Wagner, H. Gg.; Zabel, F. *Ber. Bunsen-Ges. Phys. Chem.* **1974**, *72*, 705.
(37) Teitel'boim, M. A.; Vedeneev, V. I. *Kinet. Catal*. **1986,** *26*, 1119.
(38) Tsai, C.; Belanger, S. M.; Kim, J. T.; Lord, J. R.; McFadden, D. L. *J. Phys. Chem*. **1989**, *93*, 1916.
(39) Kennedy, R. C.; Levy, J. B. *J. Phys. Chem*. **1972**, *76*, 3480.
(40) Heicklen, J. *Adv. Photochem*. **1988**, *14*, 177.
(41) Maricq, M. M.; Szente, J. J.; Khitrov, G. A.; Francisco, J. S. *Chem. Phys. Lett*. **1992**, *199*, 71.
(42) Glanzer, K.; Maier, M.; Troe, J. *J. Phys. Chem*. **1980**, *84*, 1681.
(43) Ainagos, A. F. *Kinet. Catal*. **1991**, *32*, 720.
(44) Warnatz, J. In *Combustion Chemistry*; Gardiner, W. C., Jr., Ed.; Springer-Verlag: New York, 1984.
(45) Bauer, S. H.; Javanovic, S. *Int. J. Chem. Kinet*. **1998**, *30*, 171.